

THE IMPACT OF GALAXY CLUSTER MERGERS ON COSMOLOGICAL PARAMETER ESTIMATION FROM SURVEYS OF THE SUNYAEV-ZEL'DOVICH EFFECT

DANIEL R. WIK AND CRAIG L. SARAZIN

Department of Astronomy, University of Virginia, P.O. Box 400325, Charlottesville, VA 22904-4325; drw2x@virginia.edu, cls7i@virginia.edu

PAUL M. RICKER

Department of Astronomy, University of Illinois, 1002 W. Green St., Urbana, IL 61801; pmricker@uiuc.edu

AND

SCOTT W. RANDALL

Harvard-Smithsonian Center for Astrophysics, 60 Garden St., Cambridge, MA, 02138; srandall@cfa.harvard.edu

Draft version October 31, 2018

ABSTRACT

Sensitive surveys of the Cosmic Microwave Background (CMB) will detect thousands of galaxy clusters via the Sunyaev-Zel'dovich (SZ) effect. Two SZ observables, the central or maximum and integrated Comptonization parameters y_{\max} and Y , relate in a simple way to the total cluster mass, which allow the construction of mass functions (MFs) that can be used to estimate cosmological parameters such as the ratio of the average matter density to the critical density Ω_M , the normalization of the spectrum of initial density perturbations σ_8 , and the dark energy equation of state parameter w . However, clusters form from the mergers of smaller structures, events that can disrupt the equilibrium of intracluster gas upon which SZ- M relations rely. From a set of N-body/hydrodynamical simulations of binary cluster mergers, we calculate the evolution of Y and y_{\max} over the course of merger events and find that both parameters are transiently “boosted,” primarily during the first core passage. We then use a semi-analytic technique developed by Randall et al. (2002) to estimate the effect of merger boosts on the distribution functions YF and yF of Y and y_{\max} , respectively, via cluster merger histories determined from extended Press-Schechter (PS) merger trees. The scatter in the Y - M and y_{\max} - M relations from merger boosts are found to be $\sim 2\%$ and 25–30% respectively. To determine Ω_M , σ_8 , and w , the boosted and nonboosted YF s and yF s are fit with analytic PS distributions as a function of redshift. We find that boosts do not induce an overall systematic effect on YF s, and the values of Ω_M , σ_8 , and w (assumed constant) were returned to within 2% of values expected from the nonboosted YF s. The boosted yF s are significantly biased, however, causing Ω_M to be underestimated by 15–45%, σ_8 to be overestimated by 10–25%, and w to be pushed to more negative values by 25–45%. We also fit YF as a function of redshift to cosmological models in which the dark energy parameter w varied with redshift to assess the effects of mergers on the inferred change in w with redshift. The values of Ω_M , σ_8 , and the low-redshift value of w (w_0) were again reproduced to within 2%. For the largest change in w with z , which occurred between $z = 0$ and $z = 1$ for the models assumed, it was increased by about 0.04. Although this is twice as large as the merger effect on a constant value of w , it is still reasonably modest. We confirm that the integrated SZ effect, Y , is far more robust to mergers than y_{\max} , as previously reported by Motl et al. (2005) and similarly found for the X-ray equivalent Y_X (Kravtsov et al. 2006; Poole et al. 2007), and we conclude that Y is the superior choice for a mass proxy when using SZ observations of galaxy clusters to constrain cosmological parameters.

Subject headings: cosmic microwave background — cosmological parameters — galaxies: clusters: general — hydrodynamics — intergalactic medium — large-scale structure of universe

1. INTRODUCTION

The evolution of galaxy cluster abundance traces the massive end of the spectrum of initial density fluctuations and therefore is sensitive to cosmological parameters such as the ratio of the average matter density to the critical density $\Omega_M \equiv 8\pi G\bar{\rho}/(3H_0^2)$, the normalization of the power spectrum of initial density fluctuations σ_8 , and the dark energy equation of state parameter w , equal to the ratio of the pressure to the energy density of dark energy. Here, H_0 is the Hubble constant and $\bar{\rho}$ is the average density in the universe. This sensitivity exists due to an exponential turnover at high masses in the mass func-

tion (MF) of clusters, which can be predicted from a well-established theoretical framework (e.g. Henry & Arnaud 1991; Kitayama & Suto 1996; Haiman et al. 2001). However, only gravitational lensing, which remains observationally challenging, directly measures the total mass of clusters. In order to get masses for the large number of clusters needed to construct the MF, it is often necessary to use a more observationally accessible quantity, such as the temperature or luminosity of X-ray emitting intracluster gas, from which the mass can be determined via some physical model. Relations between cluster mass and such a proxy typically require the gas

to be in virial equilibrium; however, many processes are known that can disrupt the gas, including cluster mergers (Ricker & Sarazin 2001, hereafter RS; Ritchie & Thomas 2002; Poole et al. 2006) and AGN jet-blown radio bubbles (McNamara et al. 2005).

There are many ongoing and planned surveys of clusters using the Sunyaev-Zel’dovich (SZ) effect (Sunyaev & Zel’dovich 1972; Birkinshaw 1999), which has the advantage of being effectively redshift-independent. The SZ effect is proportional to the integral of the electron pressure along the line of sight and can be characterized by the Comptonization parameter

$$y \equiv \frac{\sigma_T k_B}{m_e c^2} \int n_e T_e dl \propto \int P_e dl, \quad (1)$$

where n_e is the electron number density, T_e is the electron temperature, P_e is the electron pressure, and l is the distance along the line of sight. The actual SZ flux, measured as a decrement or increment in the Cosmic Microwave Background (CMB), depends on frequency and is subject to relativistic effects for high temperature plasmas (for a review see Rephaeli 1995). Because we do not want to tie our results to any particular observational project, we use the frequency-independent Comptonization parameter in the following study, as has been standard in the literature. Also, we ignore any relativistic corrections as they are only relevant for the most massive clusters and because they modify y in a complicated way that depends on frequency.

In general, SZ observations will give an image of the SZ effect or y across the cluster. While specific values of y , for example the central or maximum value for a cluster (hereafter y_{\max}), are not expected to be a particularly robust proxy for the mass, the integrated Comptonization parameter Y displays a tighter correlation with mass (Reid & Spergel 2006). This is defined as

$$Y = \int y dA = d_A^2 \int y d\Omega, \quad (2)$$

where A is the projected surface area of the cluster on the sky, Ω is the solid angle, d_A is the angular diameter distance to the cluster, and the integral is over the entire cluster on the sky. Because the integrated Comptonization parameter is a global quantity, proportional to $\int P_e dV$ or the thermal energy content of the electrons, it should be less sensitive to non-equilibrium processes, which tend to be more localized in cluster cores. The usefulness of SZ surveys to constrain cosmological parameters has already been discussed extensively (e.g., Carlstrom et al. 2002; Haiman et al. 2001; Holder et al. 2001).

As with X-ray proxies for mass, the regularity of an $SZ-M$ correlation relies on the fact that many clusters are energetically close to equilibrium. However, dynamically unrelaxed clusters should add scatter to this correlation. One mechanism known to disrupt the gas is cluster mergers, a direct consequence of hierarchical structure formation. How mergers affect the state of the gas will depend on the details of the individual mergers and their frequency, both of which depend on the cosmological model. To assess the utility of a mass proxy, such as the SZ effect, we need to quantify how mergers will affect the observed MF and consequently the estimation

of cosmological parameters.

Current cosmological simulations, which accurately trace the collapse of structure and thus the merger history of clusters, cannot yet build the large samples of clusters at sufficient numerical resolution to constrain fundamental parameters and assess any potential bias due to mergers – though this approach is becoming viable (e.g., Hallman et al. 2007). Typically, N-body cosmological simulations of dark matter are re-simulated to include various types of gas processes such as “preheating,” radiative cooling, and AGN feedback, from which the scatter to an observed $SZ-M$ correlation can be estimated. Depending on the resolution of the re-simulated hydrodynamic grid, these studies produce samples of ~ 10 (Nagai 2006; Bonaldi et al. 2007) to ~ 100 (Motl et al. 2005; da Silva et al. 2004) clusters. Based on similar samples of simulations, Kravtsov et al. (2006) have defined an SZ-like X-ray observable, Y_X , which they have shown to be robust to nonequilibrium gas physics with cosmological simulations. Though suited to understanding the physical processes that add statistical scatter to $SZ-M$ or similar relations, these samples are too small to assess the effect of the scatter on the determination of cosmological parameters, especially the effect of relatively rare, major merger events on the mass estimate of similarly rare massive clusters. To include these rare events and focus expressly on the role of mergers on $SZ-M$ relations and cosmological parameter estimates, we take a semi-analytic approach that avoids simulating every possible merger within a cosmological framework.

Specifically, we carefully examine the evolution of the SZ observables Y and y_{\max} for a discrete set of detailed N-body/hydrodynamical simulations of binary cluster mergers, generalize the results by identifying and parameterizing the major transient features, or boosts, and then apply these boosts to the merger histories of many clusters generated semi-analytically via computationally cheaper merger trees. We closely follow the methodology of Randall et al. (2002, hereafter RSR), who similarly investigated the effect of merger boosts on the X-ray observable mass proxies L_X and T_X , the X-ray luminosity and temperature respectively, and the bias such boosts induce upon estimates of Ω_M and σ_8 from the inferred MFs.

To assess the impact of a particular world model or cosmology on our results, we consider a “flat” cosmology with a cosmological constant, i.e. the Λ CDM concordance model, along with an “open” and Einstein-de Sitter (“EdS”) world model for comparison; the relevant parameters are summarized in Table 1. The dark energy equation of state and its evolution are only examined for the flat universe. The Hubble constant is parameterized as $100 h$ km/s/Mpc throughout.

In this paper, we assess the transient boosting of the SZ observables Y and y_{\max} during cluster mergers, and the systematic influence of mergers on cosmological parameter values derived from inferred cluster MFs. In § 2 we describe the binary cluster merger simulations from RS and the evolution of Y and y_{\max} during mergers. In § 3 we discuss the generation of cluster merger histories from merger trees created via the extended Press-Schechter formalism (Press & Schechter 1974; Lacey & Cole 1993), fit analytic functions that describe the transient behavior of merger boosts in the simulations, and generalize these

functions to the entire family of possible mergers. In § 4 the effect of boosts on the SZ– M relations are analyzed, in § 5 the distribution function proxies for the MF and the effect of boosts on them are described, and in § 6 the distribution functions are used to assess the impact of mergers on the cosmological parameters Ω_M , σ_8 , and w . Our results are discussed and summarized in § 7.

2. MERGER SIMULATIONS

To infer the effect of mergers on the SZ properties of clusters, detailed N-body/hydrodynamical simulations of every conceivable combination of cluster mass and impact parameter would be ideal. A realistic alternative is to use a small but representative set of simulated mergers (RS) and interpolate or extrapolate from them the expected behavior of SZ observables for any set of merger parameters.

A detailed description of the simulations can be found in RS. Eight simulated binary cluster mergers were available with 3 mass ratios $M_>/M_< = 1, 3, \text{ and } 6.5$ each for 3 impact parameters $b = (0, 2, 5)r_s$ except the $M_>/M_< = 6.5, b = 2r_s$ case. Here r_s is the scale radius in the NFW profile for the more massive cluster (Navarro et al. 1997). In all simulations, the less massive cluster’s mass was fixed at $M_< = 2 \times 10^{14} M_\odot$. Note that the $M_>/M_< = 6.5$ simulation runs are not specifically mentioned in RS, although they were generated by the same means as the other simulations.

2.1. Equilibrium Y – M and y_{\max} – M Relations

To compare the SZ properties of merging clusters with those of similar clusters that are not undergoing mergers, we need an equilibrium SZ– M relation. The theoretical models of clusters used in RS are designed to represent observed, non-cooling flow clusters and to have X-ray temperatures typical of present day “rich” clusters. These initial conditions therefore include “preheating” and radiative cooling, though radiative cooling is ignored as a dynamic process as the cooling timescale is designed to exceed a Hubble time. Though cooling is absent in the RS mergers, our results for y_{\max} generally agree with a similar set of cluster simulations (Poole et al. 2007) that do include radiative cooling. In any case, we are interested in the *change* of Y or y_{\max} due to mergers and not in precisely characterizing the equilibrium state of clusters. To accurately assess the relative effect of mergers on the SZ effect, we take the initial clusters in RS as our equilibrium clusters, which should correspond well to actual clusters since they were built to resemble observed, relaxed clusters.

Self-similar scaling relations derived from virial arguments (da Silva et al. 2004; Cohn & Kadota 2005) give $Y \propto M^{5/3} f_g$, where M is the virial mass and f_g is the gas mass fraction. For masses $M \gtrsim 10^{14} M_\odot$, $f_g \propto M^{1/3}$ though f_g steepens at smaller masses. This general trend of increasing f_g with mass has been observed for relaxed, nearby clusters (Vikhlinin et al. 2006). Assuming all clusters have similar density profiles, we find that $y_{\max} \propto M f_g$. For the initial clusters in the simulations, we calculate exact solutions for Y and y_{\max} :

$$Y = 0.210 \left(\frac{M}{10^{15} M_\odot} \right)^2 \left(\frac{r_s}{\text{kpc}} \right)^{-1} f_g h^{-2} \text{ Mpc}^2, \quad (3)$$

$$y_{\max} = 8.84 \times 10^3 \left(\frac{M}{10^{15} M_\odot} \right)^2 \left(\frac{r_s}{\text{kpc}} \right)^{-3} f_g. \quad (4)$$

Here, r_s and f_g are found numerically (equations (20)–(23), RS). Over the range of cluster masses we consider, Y and y_{\max} scale approximately as $Y \propto M^2$ and $y_{\max} \propto M^{1.3}$.

In practice, we fit the numerical solutions for $Y(M)$ and $y_{\max}(M)$ each to a power law times a 13 degree polynomial. The high order of the polynomial is required primarily because we need the derivatives of the function to compute the Y and y_{\max} distribution functions (YF and yF respectively). The fractional error in the derivatives of the fits is $\lesssim 1\%$ for both $Y(M)$ and $y_{\max}(M)$, and better than that for the fits themselves.

2.2. Merger Boosts to Y and y_{\max}

2.2.1. Generating Y and y_{\max} from the Simulations

For each simulation in RS, the behavior of the X-ray temperature and luminosity was calculated (see RS, Figures 5 & 8) as a function of time. We would like similar curves for Y and y_{\max} ; however, these quantities were not calculated during the simulations, so we need to evaluate them from saved 3D “snapshots” of the simulation grid in order to recreate the evolution with time. For most of the runs, 40 to 60 snapshots were saved fairly regularly over the 14 Gyr the mergers were followed. From the gas pressure distribution, the Comptonization parameters can be calculated individually for each snapshot and combined to trace the evolution of Y and y_{\max} during the merger.

Simulated SZ images for any orientation can be generated for each snapshot. As an example, Figure 1 shows 100×100 pixel images from 2 snapshots of the $M_>/M_< = 3, b = 2r_s$ merger. For both of these images, our line-of-sight is oriented at 45° to the merger axis and rotated 45° azimuthally from the merger plane. In this particular example, the clusters are seen just before and just after the first core crossing, which generally corresponds to the maximum transient enhancement of both Y and y_{\max} . Note that while the images look qualitatively similar, the scale of the image after core passage is twice that of the pre-core passage snapshot, suggesting that both Y and y_{\max} should get “boosted” during a merger event.

To compute $Y = \int y dA = \frac{\sigma_T}{m_e c^2} \int P_e dV$, we simply add up the pressure in each computational cell weighted by the cell volume so that $Y = \frac{\sigma_T}{m_e c^2} \sum_i P_{e,i} \Delta V_i$, where

the sum is over all the cells in the 3D grid. We do not restrict the integration to the virial radius r_{200} or r_{500} as in other cases where Y has been modeled (da Silva et al. 2004; Motl et al. 2005) for several reasons. First, the initial conditions for the simulated clusters cut off the pressure and density profile at the virial radius, so these definitions are at least initially equivalent. Also, during the merger there is no such well-defined radius as the gas is interacting violently. However, nearly all of the contribution to Y comes from gas inside the virial radius: 99.5% initially and 95% after the clusters have merged and equilibrated.

For each snapshot of each merger simulation, values of y_{\max} are computed for 339 orientations of the merger

relative to our line of sight. Because the effects of the merger on the value of y_{\max} tend to vary the most near the merger axis, we more finely sampled the viewing angles in this direction. The orientations sampled with respect to the merger axis are uniformly spaced in $\sin\theta$, where θ is the polar angle, such that $\Delta\sin\theta = 1/15$. The sampling of the azimuthal angle ϕ is varied, to ensure relatively even spacing, as $\Delta\phi = 8^\circ/\sin\theta$. To determine y_{\max} for each merger, snapshot, and orientation, values of y were computed by integrating along 16 lines of sight (equation (1)), on a 4x4 grid, to form an SZ image of the cluster as seen from that orientation. The grid was then recentered on the maximum value of y and reduced in scale by a factor of 3.5, and y was calculated again. This procedure was repeated until the maximum value on the grid varied by less than 0.1% compared to the value from the previous iteration, and this y is adopted as y_{\max} .

2.2.2. Correcting for Mass Loss Outside the Grid

During each merger, some gas is flung out to large radii and lost from the simulation due to the finite size of the computational grid and outflow boundary conditions at the grid edge. Of course, once the gas is outside the simulation grid, it is permanently lost. Noticeable amounts of gas do not leave the grid until after the first core passage. Since we are mainly interested in the times when the merger boost is large, which occurs near the peak associated with first core passage, our results are not particularly affected by the lost gas. At late times, however, after the clusters have merged, Y remains below the expected value for a cluster with mass $M_{\text{total}} = M_{<} + M_{>}$. Since at these cluster masses $Y \propto M^2$ and $y_{\max} \propto M^{1.3}$, we correct for the lost gas by taking

$$Y = \left[\frac{M_{\text{gas}}(t=0)}{M_{\text{gas}}(t)} \right]^2 Y_{\text{calc}}, \quad (5)$$

and

$$y_{\max} = \left[\frac{M_{\text{gas}}(t=0)}{M_{\text{gas}}(t)} \right]^{1.3} y_{\text{calc}}. \quad (6)$$

Here, Y_{calc} and y_{calc} are the integrated and maximum SZ parameters calculated by integration over the grid prior to this correction. The correction is small; over the duration of the first peak in Y , which is much longer than the peak in y_{\max} , less than 5% of the gas has been lost from the grid.

In fact, some of the lost gas exits the grid near to or above escape velocity, assuming a collisionless ballistic trajectory, so correcting for its loss may seem inappropriate. The majority of the gas, except during the short period after the first core passage, effectively leaks out of the grid due to a lack of pressure support at the simulation boundary. This artificially lower pressure propagates inward, requiring the correction we apply; otherwise, the boost will be slightly underestimated. After clusters have formed in cosmological numerical simulations, the gas fraction at the virial radius is generally 10% below the cosmic baryon fraction (Crain et al. 2007; Eke et al. 1998), perhaps indicating that up to $\sim 5\%$ of the gas has been ejected, given that 5% of the baryons are in stars. The simulations of RS we utilize cannot accurately follow the merger to its true final state and so we cannot address the question of true gas ejection from

clusters after merger events. However, the initial simulated clusters are constructed to match observed clusters with realistic gas fractions, so if gas is in fact lost, that effect is intrinsically included by RS and the resultant boosts in Y and y_{\max} . Our conclusions are not drawn from any late time evolution in the simulations, nor do we investigate the true post-merger state of clusters.

Additionally, we correct Y for the slight evolution at large radii in the relaxed, pre-merger profiles of the simulated clusters. Because the integrated Comptonization parameter is inversely proportional to a low power of cluster radius due to $Y \propto n_e$, the outer parts of a cluster contribute significantly to its overall value, as compared to L_X , which is proportional to n_e^2 . The lower pressure in the outer regions can affect Y because there is more volume at large radii, even though y_{\max} remains unaffected. We observe a slight drop in the pressure profile outside the central core over time before the individual clusters begin to interact, which is likely due to the artificial truncation of gas at the virial radius – gas at this boundary is not in hydrostatic equilibrium in the simulations and will flow outward, and the loss of pressure support will travel inward, readjusting the profile as the system tries to establish hydrostatic balance. While for the least massive cluster this effect is hardly noticeable, the magnitude of the effect increases with total cluster mass. Fortunately, the effect on $Y(t)$ appears to be linear in time, so we correct the time evolution of Y such that Y is forced to be constant before the clusters begin to interact, normalized to $Y(t=0)$.

2.3. Evolution of y_{\max} and Y During Mergers

In Figure 2, Y and y_{\max} are shown as a function of time for the merger simulations including the corrections described in § 2.2.2. For y_{\max} , the plot is shown for a viewing orientation at 90° to the merger axis and in the merger plane. The maximum boost for the head-on collision in y_{\max} is nearly a factor of 10, while the boost in Y is always less than a factor of 2, though the duration of the boost in Y is much longer than that for y_{\max} . Motl et al. (2005) report a maximum boost factor in y_{\max} of 20 in cosmological simulations re-simulated to include gas hydrodynamics, twice the amount of boosting we find, though their result could be due to an artificially high central temperature in their pre-merger clusters (Loken et al. 2002). However, it is more likely the enhanced boost is due to the natural inclusion of multiple mergers and constant accretion along filaments, which are not included in binary merger simulations. For example, a triple merger between 2 equal mass clusters and a third subcluster with a tenth of one of their masses should yield a boost factor of 20, extrapolating our results to such a case. Additional pressure due to bulk motions within the pre-merger clusters, producing stronger shocks, may also lead to a larger boost. Globally, the temperature profile of the initial clusters in RS agrees well with those clusters assembled in cosmological simulations (Loken et al. 2002), so the precise origin of the discrepancy is unclear. However, our boost factors are confirmed in a recent set of binary cluster mergers (Poole et al. 2006), in which Poole et al. (2007) find y_{\max} to be boosted by a factor of ~ 10 (see their Figure 7).

Essentially, y_{\max} traces the densest parts of clusters, which are the cores. These remain reasonably intact until

near the time of first core crossing, which makes the peak in y_{\max} relatively narrow. On the other hand, Y involves a sum of all the gas, so it begins to get boosted as soon as gas at large radii starts to interact, long before the cores approach, and the boost lasts longer, as gas in the outer regions needs more time to re-equilibrate. The time evolution of y_{\max} is qualitatively similar to that found by RS for the X-ray temperature and luminosity, quantities that are also dominated by the cores of clusters due to the fact that the X-ray emissivity depends on the square of the density.

The plots of the evolution of Y already indicate that this parameter will not be strongly affected by mergers. First, the boosts in Y are smaller than in y_{\max} . Second, the boosts are not large compared to the equilibrium effect of increasing the mass. Assuming $Y \propto M^2$, the boost factor B needed to exceed the final equilibrium value of Y_{final} is $B > \frac{Y_{\text{final}}}{Y_1 + Y_2} = \frac{(M_1 + M_2)^2}{M_1^2 + M_2^2}$. For equal mass mergers, this condition gives $B > 2$, and from Figure 2 it is clear the boost factor is always < 2 . If Y is used as a proxy to determine the mass of a cluster, the resulting value during the merger will nearly always lie between the individual initial masses of the subclusters and the final total mass. In a certain sense, this only affects the definition of when the cluster has merged, and the applicable mass, and does not represent a real bias. We find that other mass ratios can boost Y beyond the final equilibrium value, but only by factors slightly larger than unity.

3. MERGER TREES

Structure formation and evolution are most easily traced through the mass function (MF) of dark matter halos, $n(M, z)$, where $n(M, z)dM$ gives the number of halos per unit comoving volume with masses in the range $M \rightarrow M + dM$. Currently, the MF for a given cosmology at a given redshift can be found most accurately from numerical N-body simulations (Springel et al. 2005). While accessing the results of these simulations has become more feasible (e.g., Lemson & Springel 2006), a semi-analytic approach to obtaining the MF proves more practical, especially since we are concerned with the relative effect of merger boosts on the underlying MF and not the precise nature of the MF itself. We follow the PS formalism, which agrees with the MF found in numerical simulations, especially at higher masses (Bryan & Norman 1998); specifically, we use extended Press-Schechter theory as developed in Bond et al. (1991) and Lacey & Cole (1993) and applied in RSR. Though the PS formalism fails to reproduce the MF found in numerical simulations at very high redshifts and low cluster masses (see, e.g., Sheth & Tormen 1999; Lukić et al. 2007), it is more than sufficient over the redshifts ($z = 0 \rightarrow 2$) and masses ($M = 10^{14} \rightarrow 10^{16} M_{\odot}$) of interest here.

Press & Schechter (1974) give the MF at some redshift z as

$$n_{PS}(M, z)dM = \sqrt{\frac{2}{\pi}} \frac{\bar{\rho}}{M} \frac{\delta_c(z)}{\sigma^2(M)} \left| \frac{d\sigma(M)}{dM} \right| \exp \left[-\frac{\delta_c^2(z)}{2\sigma^2(M)} \right] dM \quad (7)$$

where $\sigma(M)$ is the current rms density fluctuation within a sphere of mean mass M , and $\delta_c(z)$ is the critical linear overdensity required for a region to collapse at redshift

z . The derivation of this expression assumes that halos grow from Gaussian density fluctuations that have larger amplitudes on smaller scales. Structure then forms hierarchically, with small halos collapsing first and merging to form larger halos. In this scenario, the highest mass halos, observed as clusters of galaxies, form most recently and should be most affected by merger processes at the present day.

From this extended PS formalism, we follow the procedure outlined in § 3 of RSR, in which a “merger tree” is generated for a present day cluster. The merger tree traces the merger and accretion history of a cluster of mass M back in time. For each time step, a progenitor cluster of mass M_{p1} is chosen from a probability distribution (Lacey & Cole 1993, equation (2.25)), and since we only consider binary mergers, the mass of the other progenitor cluster is given by $M_{p2} = M - M_{p1}$. We will use the notation $M_>$ and $M_<$ for the larger and smaller masses of the subclusters in each binary merger. RSR in § 3.1 discusses the disadvantages of dealing solely with binary mergers; however, our set of simulated mergers does not address more complex mergers, so we have no good way to derive a boost for them. Also, boosts are most dramatic for near equal mass mergers, and in such cases additional merger participants will likely be much less massive and have a negligible effect on the resultant boosts. However, one result of ignoring multiple mergers is that the merger tree-derived MF tends to overestimate the analytic PS MF for $z > 0$. The progenitor cluster with mass M_{p2} is not taken from the PS distribution and is generally overestimated, so that the high mass end of the MF is overestimated at the expense of the very low mass end. Since we concern ourselves with the highest mass clusters, our resulting MFs will lie slightly above the analytic prediction, as illustrated in Figure 6, which we must take into account when fitting MFs in § 6.

A large number of merger trees was created with a broad span of initial cluster masses, and the distribution of the initial masses was weighted so as to give the present day mass function. From ensembles of merger trees for the cosmologies of interest, we can find the MF at any redshift, and at any redshift we have each cluster’s merger history, which can be used to determine the merger boost in some observable — in our case Y and y_{\max} .

Merger trees are a simple and computationally cheap way to simulate structure formation for a particular world model. But they are limited in that they only specify progenitor cluster masses and discrete time intervals during which the mergers occur. All the dynamics and other details of a merger, however, are absent from EPS-derived merger trees. The information needed to connect the trees to our merger simulations is the masses of the clusters, the impact parameter b of the encounter, and the time of first core passage, which we designate as the time of the merger, t_{merge} , in the merger trees. While the masses are provided by the merger trees, an appropriate b must be selected for each merger in the trees. We follow the method in § 6 of RSR, where a value for the spin parameter is chosen from a Maxwell-Boltzmann-like distribution, which represents the observed distribution from numerical simulations (Bullock et al. 2001), allowing b to be derived from the chosen spin parameter (Sarazin 2002). To determine the precise value of t_{merge} , we sim-

ply select a random time within the small discrete time step used in the merger trees, and take that time to be the instant of first core passage, since the merger could have occurred at any point within that time.

3.1. Merger Boost Histograms

As discussed in RSR, the effect of a merger boost on a cluster whose history is characterized by a merger tree can be determined from a histogram which gives the magnitude of the boost as a function of time. Since the merger trees give a statistical description of the history of cluster mergers, it is sufficient to determine the distribution histogram of boosts versus the observed time t_{obs} . The form of the histogram reduces the details contained in the curves in Figure 2 to a simpler, one-to-one function that can be fit by the merger parameters $M_{<}$, $M_{>}$, and b . In the fits, we scale the impact parameter b by the core radii of the two merging clusters, $b' = b/(r_{c<} + r_{c>})$ and the time by the ratio of the virial radius of the more massive cluster to the gas sound speed, t_{sc} . A more detailed explanation of these scalings is given in § 5.3 of RSR.

3.1.1. Fitting Y Histograms from Simulations

The left panel of Figure 3 shows the cumulative time spent by the system above any given value of Y for the $M_{>}/M_{<} = 1$ merger simulations. We use cubic spline interpolation of the boost curves in the left panel of Figure 2 to produce a smoothly varying histogram. In RSR, the T_X and L_X boost histograms were well-fit by hyperbolas parameterized by the equations given in their Appendix B. We find hyperbolas also well-describe the Y histograms, and we use the same parameterization as RSR with only a minor change given in Appendix A.

3.1.2. Fitting y_{max} Histograms from Simulations

The procedure for y_{max} is slightly more complicated due to the orientation-dependence of the central Comptonization parameter. The evolution of the maximum value of y as a function of viewing angle varies more dramatically near the merger axis than perpendicular to it. As noted in § 2.2.1, for each merger simulation, the evolution of y_{max} with time was calculated for 339 orientations, sampling more finely around the merger axis. Because y_{max} really traces the cluster cores, the peaks in the curves are larger and have shorter durations. As a result, we found that simple interpolation did not sufficiently sample the peaks, so we use a superposition of Gaussians to fit the shape of the boost as a function of time.

The merger trees contain no information about the orientation of the cluster mergers, and we assume an isotropic distribution relative to our line-of-sight. For our grid of 339 viewing angles, the probability of any one orientation is determined by the solid angle of that grid cell. We weight each orientation by this solid angle divided by 4π . All 339 $y_{\text{max}}(t)$ curves, weighted by their probability of being observed, are used to construct a histogram like those described in § 3.1.1. The histograms for the $M_{>}/M_{<} = 1$ runs are shown in the right panel of Figure 3. Since these histograms include the distribution of merger boosts for all orientations of the line of sight, the boosts need to be normalized to the pre-boost

value of y_{max} for some fixed orientation. The boosts in the right panel of Figure 3 were taken relative to the pre-boost y_{max} as observed 90° to the merger axis and in the merger plane. Note that this is the same orientation assumed in the right panels of Figure 2.

Because the y_{max} histograms include the results from many different orientations, the high boost ends of the histograms decline more slowly with time than for Y or L_X or T_X . A different function is thus used to fit these histograms (see Appendix A).

3.2. Generalizing Merger Boosts for Arbitrary Mass Ratio and Impact Parameter

As in RSR, the parameters of the fits to the boost histograms were fit to simple functions of the masses and impact parameter in the merger. The forms of these functions were chosen so as to have the correct asymptotic forms (e.g., in the limit of large $M_{>}/M_{<}$). The free parameters of these functions were chosen to best fit the histograms from all 8 simulation runs. The values of these parameters are given in Table 5 (below in the Appendix) for the Y and y_{max} histograms.

The maximum fractional error in the fits to the boost simulation data for Y is $< 3\%$ except for the 2 runs with $M_{>}/M_{<} = 6.5$. Here, the evolution of the pressure distribution in the more massive cluster before collision dominates the time evolution of Y (see § 2.2.2). The fits overestimate the boosts for the $M_{>}/M_{<} = 6.5$ simulations; however, the boosts themselves are small in this case, and the errors are still $< 10\%$.

For the y_{max} fits, the average fractional error is typically 4%, and the maximum error is $< 10\%$. We found that the time sampling for the $M_{>}/M_{<} = 3, b = 2r_s$ simulation run was too sparse around the boost to strongly constrain the shape of the y_{max} histogram, so we did not use this run in our fits.

3.3. Adding Boosts to Merger Trees

With the fitted forms for the histograms for the strength of a boost versus time as a function of the masses of the merging subclusters $M_{<}$ and $M_{>}$ and the impact parameter b , the boosted values of Y or y_{max} can easily be found for clusters from their past merger histories given by the merger trees. For any redshift or observed time, t_{obs} , we search back through a cluster's merger tree and for every merger event, we find the boosted value of Y or y_{max} for that merger. If the boosted Y or y_{max} exceeds the value given by our equilibrium equations (3) and (4) for the mass of the cluster at t_{obs} , then we assign the boosted value to that cluster's observed Y or y_{max} ; otherwise it acquires its equilibrium value. Boosted values less than those given by the equilibrium equations are not allowed because the analytic fits from which boost factors are derived poorly describe the histograms, such as those shown in Figure 3, for negative and small positive boosts. While the discrepancy between the simulation-based histograms and the analytic fits for small boosts leads to an underestimate of the number of these clusters, we are primarily concerned with the more dramatic effects caused by large boosts, which are well-described by the fits.

Once clusters observed at some redshift are assigned values of Y and y_{\max} based on each cluster’s merger history, we can evaluate the robustness of the $Y - M$ and $y_{\max} - M$ relations. The top panels of Figures 4 and 5 show Y and y_{\max} versus mass for clusters in our merger trees at $z = 0$ and $z = 1$. Most clusters have nearly unboosted values of Y and y_{\max} , while the number of clusters that deviate from either SZ- M relation drops roughly exponentially with the strength of the boost. We find that $\sim 15\%$ of clusters are boosted in y_{\max} by $\gtrsim 15\%$ and in Y by $\gtrsim 0.1\%$. Note that the scatter in Figures 4 and 5 is due entirely to merger boosts and does not include observational error or scatter related to other physics.

As expected, many clusters are found to have significantly boosted values of y_{\max} , which overestimate the actual masses. However, there are almost no “boosts” to Y in Figure 4. Instead, we see clusters scattered *below* the $Y - M$ relation, as is also seen, though to a lesser extent, in Figure 5. Clusters that fall below the $Y - M$ relation were “observed” after a merger (after the peak of the boost), but before virialization. It should be noted that, according to § 3.3, a boost is only applied if it gives a Y or y_{\max} greater than its equilibrium value *before* the merger, while in Figures 4 and 5 the mass is taken to be the final, or merged, mass of the clusters. So, though clusters can never fall below their pre-merger equilibrium relation in our formulation, a boosted cluster may fall below its post-merger value. The scatter below the $y_{\max} - M$ relation is less pronounced due to the shorter period when the SZ effect is below the eventual equilibrium value (see Figure 2). This feature is a general characteristic of observing a recent post-merger cluster and will be difficult to identify as such in an actual survey, and will likely affect the normalization of either SZ- M relation.

In order to quantify the effect of mergers on the SZ versus mass relations, we fit power-law functions of the form

$$Y = A \times 10^{-5} h^{-2} \left(\frac{M}{10^{15} M_{\odot}} \right)^{\alpha} \text{ Mpc}^2, \quad (8)$$

or

$$y_{\max} = A \times 10^{-5} \left(\frac{M}{10^{15} M_{\odot}} \right)^{\alpha}, \quad (9)$$

to all of the clusters with $Y > 10^{-5} h^{-2} \text{Mpc}^2$ or $y_{\max} > 10^{-5}$. We estimate the scatter with respect to the best fit, σ_{fit} , and also the scatter and offset with respect to the actual equilibrium relations for the SZ effect (equations (3) and (4)), σ_{eq} . We define the scatter as

$$\sigma_{\text{fit}}^2 = \frac{\sum_i (y_i - y_{\text{fit},i})^2 / y_{\text{fit},i}^2}{N - 1}, \quad (10)$$

and σ_{eq} is similarly defined, except $N - 1$ is replaced by N . The coefficients A and α of the fits along with the scatter are given in Table 2. The subscripts “b” and “nb” refer to clusters including merger boosts, and not including these boosts (where the SZ properties are given by the equilibrium relations). Note that we consider a logarithmic distribution as in § 5 for the cluster masses, so that the fits in Table 2, as well as the points in Figures 4 and 5, do not reflect the actual MF of clusters.

Because the relative strength of boosts is mainly a function of mass ratio and is only weakly dependent on the absolute masses of the merging clusters, clusters are boosted somewhat uniformly in Y and y_{\max} across masses, which tends to change the normalization of the fit, A , and only to a lesser extent the slope, α . The inclusion of merger boosts, in the case of y_{\max} , could either flatten or steepen the slope. The local mass function is flatter at the low-mass end, so low-mass clusters experience more high-mass-ratio mergers overall than high-mass clusters, thus flattening the $y_{\max} - M$ relation. However, when both minor and major mergers are considered, at any given time the high-mass clusters are undergoing more merger events (see the relative change in yF over time for low- and high-mass clusters in Figure 6). Thus, at any given time a higher-mass cluster has a greater probability of finding itself in the midst of a merger of some type. If the mass function is oversampled at the high-mass end, this effect tends to steepen the $y_{\max} - M$ relation. Because our cluster sample has a uniform distribution in log mass, we oversample the high-mass end relative to the low-mass end. Consequently our $y_{\max} - M$ relation does not exhibit the flattening that we would expect if our cluster sample had been drawn from the correct mass function. As Figure 5 shows, both high- and low-mass clusters exhibit the same number of large boosts, but the total number of boosted clusters is greater at higher masses. Most of the high-mass clusters with boosts have small boost factors that are difficult to see in the figure.

The boosted normalization for Y is systematically lower than the nonboosted A , but by $< 1\%$. In the case of y_{\max} , the normalization increases by $\sim 10\%$. The offsets to y_{\max} are due as much to clusters with small boost factors as to the rarer cases with very large boosts. Note that these clusters tend to be undergoing weaker mergers, which may be hard to detect. Thus, it may be difficult to expunge these clusters from SZ surveys, and the systematic shift in the y_{\max} versus mass relation may bias cluster samples. The merger-induced scatter to the fit, σ_{fit} , is $\sim 2\%$ for the $Y - M$ relation and 25-30% for the $y_{\max} - M$ relation, and is nearly independent of the cosmological world model and redshift. The scatter relative to the equilibrium relations, σ_{eq} , increases with redshift since the merger rate is higher in the past, whereas the addition of boosted clusters adjusts the normalization A to minimize σ_{fit} , so the scatter remains about constant between redshifts. Also, because there are fewer clusters that show boosts in Y , the scatter σ_{fit} is dominated by deviations of the equilibrium relation from a power-law form, which explains why σ_{eq} tends to be slightly smaller than σ_{fit} for Y .

5. DISTRIBUTION FUNCTIONS OF Y AND Y_{MAX}

We computed the distribution functions for Y and y_{\max} , which we refer to as the YF and yF , respectively. The distribution function YF is $n(Y, z)$, where $n(Y, z) dY$ gives the number of clusters per unit comoving volume at redshift z which have integrated SZ parameters in the range $Y \rightarrow Y + dY$. The yF distribution function $n(y_{\max}, z)$ is defined in an equivalent manner. To build the YF from a merger tree, we find all the clusters that exist at the “observed” redshift and assign a value of Y according to § 3.2 for the non-boosted YF

and § 3.2 for the boosted YF. A cluster with integrated Comptonization parameter Y_i is then added to a pre-determined bin YF_j such that $Y_j^{\text{bin}} \leq Y_i < Y_{j+1}^{\text{bin}}$ and appropriately weighted to convert the actual initial distribution of $z = 0$ cluster masses used in the merger trees, dN/dM^0 , to the Press-Schechter distribution n_{PS} :

$$YF_j = YF_j + \frac{n_{PS}(M^0, z = 0)}{\frac{dN}{dM^0}(Y_{j+1}^{\text{bin}} - Y_j^{\text{bin}})} \quad (11)$$

The initial distribution dN/dM^0 is logarithmically spaced to ensure good statistics at the high mass end, where clusters are rare, and to avoid creating an excessively large number of merger trees.

For the non-boosted case, the YF or yF can be found directly from the equilibrium relations (equations (3) & (4)) and

$$n_{PS}(Y, z)dY = n_{PS}(M, z)\frac{dM}{dY}dY \quad (12)$$

$$n_{PS}(y_{\text{max}}, z)dy_{\text{max}} = n_{PS}(M, z)\frac{dM}{dy_{\text{max}}}dy_{\text{max}} \quad (13)$$

with $n_{PS}(M, z)$ from equation (7). The derivatives are found from fits to the equilibrium relations (see § 2.1).

The agreement between the nonboosted merger tree-derived YFs (yFs) and the analytic Press-Schechter YFs (yFs) is shown in Figure 6 for the flat world model. Note that the merger trees seem to slightly overestimate the number of lower Y or y_{max} (i.e. lower mass) clusters at higher redshifts, which is due to a feature of our merger tree procedure discussed in § 3 of this work and § 3.1 of RSR.

The nonboosted and boosted YFs and yFs are also compared in Figure 6. The boosted YFs are almost identical to the nonboosted YFs. The deviations from the nonboosted YFs are not systematic and are typically of a few percent and only visible in the residual plot. The boosted yFs, however, lie systematically above the nonboosted yFs at all 3 redshifts considered. The fractional deviation increases with both cluster mass and redshift. The increase with cluster mass shows that rare events involving major mergers of moderate mass clusters compete in frequency with the number of rare, very massive clusters with large equilibrium values of y_{max} . The increase in the bias with redshift is apparently due to the higher merger rate in the past. Clearly, clusters with all values of y_{max} are getting boosted to higher y_{max} bins in the yFs over our considered range of y_{max} , which includes only the most massive clusters. Such a significant and systematic bias in the yF will affect estimates of cosmological parameters, as discussed below in § 6.

6. DETERMINING COSMOLOGICAL PARAMETERS FROM THE MERGER TREE YFS AND YFS

Although mergers strongly affect the SZ signals of a small fraction of clusters, because of the exponential high-mass drop-off in the YF and yF the effect of mergers on cosmological model fits to these distributions may be significant. To quantify this effect, we derive fits based on the analytic predictions of equations (12) and (13) to the YF and yF using both boosted and nonboosted merger trees. The differences between the best-fit cosmological parameters derived in the two cases provide an estimate

of the systematic bias introduced when merging effects are neglected.

6.1. Varying only Ω_M and σ_8

For our 3 cosmological world models, we treat the binned YFs and yFs from the merger trees as observational data and find best-fit values for the parameters Ω_M and σ_8 in equation (12) or (13). Due to a near degeneracy between Ω_M and σ_8 (Bahcall & Fan 1998) at a single redshift, we simultaneously fit YFs and yFs for two redshifts: at $z = 0$ and at either $z = 0.5$ or $z = 1.0$. While in practice SZ surveys will observe clusters in a continuous range of redshifts, choosing only 2 redshifts simplifies the fitting procedure and illustrates the effect of merger boosts on these parameters. We choose to only fit clusters above a minimum value of $Y^{\text{min}} = 10^{-5}h^{-2}\text{Mpc}^2$ or $y_{\text{max}}^{\text{min}} = 10^{-5}$. These limits are consistent with the expected detection thresholds for upcoming SZ surveys, such as the AMI, ACT, and SPT projects (e.g., Bartlett 2006), and the likely confusion limit for clusters with $M \lesssim 10^{14}h^{-1}M_{\odot}$ (Holder et al. 2007). These limits also keep our fits from being biased by the large number of clusters at low masses.

To evaluate the extent to which merger boosts affect the estimation of Ω_M and σ_8 , we compare their fitted values from the boosted YFs and yFs to the fitted values from the nonboosted YFs and yFs. We do not compare best-fit parameters to the values used to create the merger trees because the trees tend to slightly overestimate the MF, an effect which increases with redshift and is discussed in § 3. However, since we are only interested in *relative* changes to the YF or yF due to boosts in Y or y_{max} , this bias in the MF does not affect our results, though the best-fit parameters found from the nonboosted YFs or yFs may differ from the parameter values used to create the trees. Also, any bias caused by our chosen fitting method is accounted for by directly comparing the two YFs or yFs.

The best-fit values of Ω_M and σ_8 for the flat, open, and EdS cosmological world models are given in Table 3 for both Y and y_{max} . The parameter values used to create the merger trees are summarized in Table 1 for reference. In general, the results are independent of world model; cosmological parameter fits tend to be biased in the same direction by about the same amount. However, boosts to Y have almost no effect on fits to Ω_M and σ_8 ; the changes due to mergers are generally less than 1% and are not clearly systematic.

In contrast, boosts to y_{max} significantly bias the values of these parameters: Ω_M is underestimated by 15-30% and σ_8 is overestimated by 10-20%. The main effect of merger boosts is to increase the number of clusters detected in a particular yF_{*j*} bin; in other words, there is a systematic increase in the yF, as shown in the right panel of Figure 6. An overall increase in the normalization of the yF leads to an increase in the normalization of the spectrum of initial density perturbations, σ_8 . The total matter content, Ω_M , is also sensitive to the normalization, but it is nearly degenerate with $\sigma_8 \approx 0.6\Omega_M^{-1/2}$ (Bahcall & Fan 1998) at a given single redshift. However, Ω_M is more sensitive to the change in the yF over time – the greater the density of matter, the faster structure will grow. If various cosmologies with nearly identi-

cal yFs at $z = 0$ are considered, those cosmologies with smaller values of Ω_M (and thus larger values of σ_8) would produce yFs at $z > 0$ that lie above the yFs of cosmologies with larger Ω_M values. As described in § 5, merger boosts raise the yF most strongly at higher redshifts, so the change in the yF from one redshift to another is smaller than for nonboosted yFs, indicating a slower structure growth rate and therefore a smaller Ω_M . The overall effect of mergers seems to vary with redshift; Ω_M and σ_8 are found to be less biased when utilizing the yF at higher redshift ($z = 1$) even though this yF is fractionally more biased than the yFs at $z = 0$ or $z = 0.5$.

6.2. Fitting the Dark Energy Equation of State Parameter w

Clusters of galaxies have been used to constrain the equation of state parameter w of dark energy, and there are extensive plans to improve these measurements in the future using SZ surveys (e.g., Haiman et al. 2001; Weller et al. 2002). In the Λ CDM flat world model, dark energy is assumed to take the form of a cosmological constant, which has a fixed $w = -1$. Here, we assess the effect of mergers on the determination of w by allowing w to vary along with Ω_M and σ_8 in fits to the flat world model YFs and yFs, following the same procedure outlined in § 6.1. We need new analytic, nonboosted Press-Schechter YFs and yFs that incorporate $w \neq -1$, which we write as $n_{PS}(Y, z, w)$ and $n_{PS}(y_{\max}, z, w)$. The same basic form of n_{PS} can be generalized to a constant $w \neq -1$ and a slowly varying parameterization of $w(z) = w_0 + w_1 a(1 - a) = w_0 + w_1 z/(1 + z)^2$, where a is the scale factor and w_0 and w_1 are constants and w_1 is small. In a flat ($\Omega_M + \Omega_{DE} = 1$) universe, we change the expression for the growth function $D(z)$ as given in Appendix A of RSR and correct the comoving volume element dV such that

$$\left(\frac{dN}{dVdY}\right)^w = \left(\frac{dN}{dVdY}\right)^{w=-1, \delta_c(D(z,w))} \left(\frac{d_A^{w=-1}}{d_A^w}\right)^2 \left(\frac{dV^{w=-1}}{dV^w}\right) \quad (14)$$

where $\left(\frac{dN}{dVdY}\right)^{w=-1, \delta_c(D(z,w))}$ is $n_{PS}(Y, z)$ for the Λ CDM cosmology, but with the critical overdensity δ_c given by the new growth function $D(z, w)$ [equation (20) from Percival (2005) for constant w or equation (14) from Wang & Steinhardt (1998) for $w(z)$], and d_A is the angular diameter distance. The ratio of volumes is

$$\left(\frac{dV^{w=-1}}{dV^w}\right) = \left(\frac{d_A^{w=-1}}{d_A^w}\right)^2 \left[\frac{E(z, w)}{E(z, w = -1)}\right], \quad (15)$$

where $E(z, w) = [\Omega_M(1 + z)^3 + \Omega_{DE}(1 + z)^{3+3w}]^{1/2}$. The same expression applies for the yFs by replacing Y with y_{\max} and dropping the factor $\left(\frac{d_A^{w=-1}}{d_A^w}\right)^2$ from equation (14).

6.2.1. Constant $w \neq -1$

When we allow for constant values of w that are not necessarily equal to -1 , we find results qualitatively similar to what was found previously when only Ω_M and σ_8 were varied. Again, the boosted YFs give back nearly identical values for all 3 parameters to within $\lesssim 1\%$. For y_{\max} , merger boosts are found to bias the fitted values

for Ω_M and σ_8 even more strongly, underestimating Ω_M by 30-45% and overestimating σ_8 by 20-25%. Also, w is found to be more negative in the boosted yFs by 25-45%, making y_{\max} a poor proxy if one aims to constrain the nature of dark energy. These results are summarized in Table 4.

In the case of y_{\max} , the boosted yFs favor more negative values of w due to w 's impact on structure formation. The yF is overestimated to a greater extent at larger redshifts (see Figure 6), which mimics more structure in the recent ($z \lesssim 1$) past. In turn, the appearance of more collapsed structures in the past relative to the present time implies that recent structure formation was slower than it actually has been, and that structure formation in the far past was correspondingly faster. In general, if we compare the effect of different values of w on structure formation by holding the present yF fixed, a more negative w is better able to slow down cluster formation at later times as the strength of dark energy grows with the scale factor a since $\Omega_{DE} = \Omega_{DE,0}(1 + z)^{3(1+w)}/E^2(z)$. If cluster formation is slowing at the current epoch, when dark energy has recently become dominant, there must be more clusters in the recent past compared to the yF of clusters under the influence of a less negative w .

A more negative w allows for even smaller values of Ω_M to be fit to the boosted yFs, compared to its best-fit values when only Ω_M and σ_8 are varied. By anchoring the current yF, a more negative w *decreases* the influence of dark energy in the past, so Ω_M does not need to be as large to form the same amount of structure. The dark energy equation of state does not as directly affect the overall normalization of the yFs, so the bias to σ_8 remains consistent with the fixed $w = -1$ fits.

6.2.2. Slowly Varying $w(z)$

If dark energy is not due to a cosmological constant, then it is possible that its equation of state might vary. We have also determined the effect that merger boosts can have on the SZ determination of the evolution of dark energy. We only consider the effect of boosted YFs in this section, due to the difficulty of using yFs to pin down even constant values of w . Choosing the parameterization of $w = w_0 + w_1 z/(1 + z)^2$, where w_0 and w_1 are constants, we determined Ω_M , σ_8 , w_0 , and w_1 by fitting the boosted and nonboosted YFs. The validity of the form of the growth function we use for a flat universe requires that $|\frac{dw}{d\Omega_M}| \ll \frac{1}{1 - \Omega_M}$, which implies that $w_1 \ll 1$ for $w_0 \approx -1$ and $\Omega_M \approx 0.3$ (Wang & Steinhardt 1998). We do not constrain our best-fit value of w_1 according to this requirement, however, nor do we consider any other parameterization of w .

We found that w_1 was not well-constrained by fitting the YFs or yFs at only two redshifts. Thus, we simultaneously fit the distribution functions at the three redshifts $z = 0, 0.5$, and 1 . As in the constant w case, the boost-derived values of Ω_M , σ_8 , and w_0 deviated from the nonboosted values only slightly, by +0.5%, -0.2%, and +2%, respectively. The best-fit values of w_1 increased by 0.15 from the nonboosted value of -0.19 to a value for the boosted YF of -0.04. For the assumed variation of w with z , the largest change in w occurs between the present time ($z = 0$) and $z = 1$; that change is $\Delta w = w_1/4$. Thus, the merger boost effects on YF

alter the maximum change in the w by about 0.04. This is about twice as large as the effect on w_0 , but is still relatively small.

7. DISCUSSION AND SUMMARY

We have determined the effects of cluster mergers on their SZ properties, particularly the integrated Y and maximum y_{\max} Comptonization parameters. From a set of hydrodynamical/N-body simulations of cluster mergers, we determined the evolution of Y and y_{\max} over the period of interaction for mergers of various mass ratios and impact parameters, and we found that mergers temporarily “boost” both Y and y_{\max} . For y_{\max} , the boosts can be as large as an order of magnitude, although they occur for a short time (typically about half the sound crossing time of the cluster), with the largest boosts occurring near the time of first core crossing. For major mergers, the boosts in the maximum Comptonization parameter generally exceed the increase in y_{\max} when the systems have come into equilibrium.

On the other hand, the boosts in Y are smaller (less than a factor of two), although they last longer (about two sound crossing times). Most importantly, the boosts in Y for major mergers are smaller than the increases in Y when the merged clusters have come into equilibrium. Thus, one can think of the merger “boost” in Y as representing a stage in the evolution from two separate equilibrium values to the final merged value, and not really being a “boost” at all. A simple physical argument explains why the transient boosted values of Y are smaller than the final equilibrium values. From equation (2), it follows that Y is just proportional to the total thermal energy content of the electrons in the clusters, or just the total thermal energy if the electrons and ions are in equipartition. Now, a cluster merger involves the conversion of the bulk kinetic energy of the merging clusters into thermal energy. When the merger is complete, there is very little bulk kinetic energy remaining (perhaps, weak rotation or turbulence). Thus, one expects the thermal energy content of the merging clusters to be largest when they have achieved (or nearly achieved) equilibrium. Thus, the final equilibrium value of Y will tend to be larger than any transient value during the merger.

We generalized the SZ boosts to mergers of arbitrary mass ratio and impact parameter and traced the merger, and thus boost, history of clusters with redshift using the EPS merger tree formalism. In general, merger boosts induced a relatively small scatter, $\sim 2\%$, below the equilibrium Y - M relation, while mergers induced a large scatter of 25-30% above the y_{\max} - M equilibrium relation. Power-law fits to Y and y_{\max} as a function of mass show that while boosts do not affect the slope of the fit, the normalization was lowered by $< 1\%$ for Y and raised by $\sim 10\%$ for y_{\max} .

We used the merger trees to derive the distribution functions of SZ parameters, YF and yF. We found that the boosted YF was not significantly biased relative to the nonboosted YF, while the boosted yF was strongly biased above the nonboosted yF for all redshifts. In general, the size of the merger-induced bias increased with redshift and with cluster mass.

Using the YFs and yFs, we determined the best-fit values for the cosmological parameters Ω_M and σ_8 for

the flat, open, and EdS world models, and also the dark energy equation of state parameter w for the flat universe. Comparing the best-fit values of Ω_M and σ_8 for the nonboosted and boosted YF, no significant difference ($< 1\%$) was observed. In contrast, the boosts to the yF decreased the best-fit value of Ω_M by 15-30% for the flat and open world models and increased the best-fit value of σ_8 by 10-20% for all world models. These results stem mainly from an overall increase in the yFs, which pushes σ_8 to larger values, and a greater increase in the boosted yF at higher redshifts relative to lower redshifts, which pushes Ω_M to smaller values. Allowing for a constant $w \neq -1$ in the flat world model, no systematic difference in fitted cosmological parameters was found between the two sets of YFs, though the merger-induced bias to Ω_M , σ_8 , and w was exacerbated when using the yFs. We also considered a time-varying $w(z)$ for the YFs, for which Ω_M , σ_8 , and w_0 were found to be consistent with the previous results for a constant $w \neq -1$, though boosts increased the best-fit value of the dark energy evolution parameter w_1 by about 0.15. The largest change in w occurs between $z = 1$ and $z = 0$ in this model; thus, the change in w might be affected by as much as 0.04. This is about twice as large as the maximum change in the present-day value of w_0 , but still is relatively moderate.

These results agree with previous work which indicates that global observables such as Y or the equivalent X-ray/mass proxy Y_X are more robust as mass proxies than the central or maximum Comptonization parameter. For example, from semi-analytic models of the intra-cluster medium (ICM), Reid & Spergel (2006) generally find that $Y \propto f_g M^{5/3}$, equivalent to our equilibrium definition of Y , with only a small scatter due to internal physics. A number of studies have used cosmological N-body simulations and re-simulated forming clusters with various kinds of gas physics to evaluate the scatter in the y - M relations (Nagai 2006; Bonaldi et al. 2007). It is generally found that the normalization A varies significantly depending on the ICM physics, though the slope α does not. Nagai (2006) reports a scatter of 10-15% in the Y - M relation, much larger than our scatter of ~ 2 -3%. Also, Kravtsov et al. (2006) defines an X-ray observable $Y_X = T_X M_{\text{gas},500}$, which is similar to our $Y \propto \int n_e T_e dV \sim T_e \int n_e dV \propto T_e M_{\text{gas}}$; they find a scatter in the relation of 5%-7%.

While these studies intrinsically include mergers, they have limited statistics as they generally consist only of a small number of systems, ~ 10 or so. Some studies have considered somewhat larger cluster simulation samples including hundreds of clusters (Motl et al. 2005; da Silva et al. 2004) from cosmological simulations. Our results agree with their conclusions that the Y - M relation is relatively stable to mergers, unlike the y_{\max} - M relation. Motl et al. (2005) find a scatter in their Y - M relation of 3-4% and in their y_{\max} - M relation of $\sim 17\%$ at $z = 0$ due to mergers and other ICM physical processes. These results compare well with our scatter of 2% and 24%, respectively.

In a study similar to this work, Poole et al. (2007) take a suite of binary cluster merger simulations to assess the effect of various observables, including SZ parameters, on scaling relations during mergers. The evolution of y_{\max} (which they call y_o) in their simulations is qual-

TABLE 1
COSMOLOGICAL
PARAMETER VALUES USED
TO CREATE MERGER TREES

Model	Ω_M	Ω_Λ	σ_8
Flat	0.3	0.7	0.834
Open	0.3	0.0	0.827
EdS	1.0	0.0	0.514

itatively similar to our results in Figure 2 for various impact parameters and mass ratios. They also consider an integrated Comptonization parameter, but it is only integrated out to a radius r_{2500} and is thus much more dominated by core effects and not equivalent to our Y , which is effectively integrated to at least r_{200} , the virial radius.

The large number of galaxy clusters expected from upcoming SZ surveys, both locally and at potentially high redshifts, heightens the prospects that clusters could play a decisive role in the era of precision cosmology, especially if the robustness of Y as a proxy for mass is confirmed

in real cluster samples.

This work was supported in part by the National Aeronautics and Space Administration through *Chandra* awards GO5-6126X, and TM7-8010X, and through *XMM-Newton* awards NNG05GO50G, NNG06GD54G, NNX06AE76G, and NNX06AE75G, and through *Suzaku* awards NNX06AI37G, and NNX06AI44G. DRW acknowledges the support of a Virginia Space Grant Consortium graduate fellowship. We would like to thank the referee for very helpful comments.

REFERENCES

- Bahcall, N. A., & Fan, X. 1998, *ApJ*, 504, 1
- Bartlett, J. G. 2006, *ArXiv Astrophysics e-prints*, arXiv:astro-ph/0606241
- Birkinshaw, M. 1999, *Phys. Rep.*, 310, 97
- Bonaldi, A., Tormen, G., Dolag, K., & Moscardini, L. 2007, *MNRAS*, 378, 1248
- Bond, J. R., Cole, S., Efstathiou, G., & Kaiser, N. 1991, *ApJ*, 379, 440
- Bryan, G. L., & Norman, M. L. 1998, *ApJ*, 495, 80
- Bullock, J. S., Dekel, A., Kolatt, T. S., Kravtsov, A. V., Klypin, A. A., Porciani, C., & Primack, J. R. 2001, *ApJ*, 555, 240
- Carlstrom, J. E., Holder, G. P., & Reese, E. D. 2002, *ARA&A*, 40, 643
- Cohn, J. D., & Kadota, K. 2005, *ApJ*, 632, 1
- Crain, R. A., Eke, V. R., Frenk, C. S., Jenkins, A., McCarthy, I. G., Navarro, J. F., & Pearce, F. R. 2007, *MNRAS*, 377, 41
- da Silva, A. C., Kay, S. T., Liddle, A. R., & Thomas, P. A. 2004, *MNRAS*, 348, 1401
- Eke, V. R., Navarro, J. F., & Frenk, C. S. 1998, *ApJ*, 503, 569
- Haiman, Z., Mohr, J. J., & Holder, G. P. 2001, *ApJ*, 553, 545
- Hallman, E. J., O’Shea, B. W., Burns, J. O., Norman, M. L., Harkness, R., & Wagner, R. 2007, *ApJ*, 671, 27
- Henry, J. P., & Arnaud, K. A. 1991, *ApJ*, 372, 410
- Holder, G., Haiman, Z., & Mohr, J. J. 2001, *ApJ*, 560, L111
- Holder, G. P., McCarthy, I. G., & Babul, A. 2007, *MNRAS*, 382, 1697
- Kitayama, T., & Suto, Y. 1996, *ApJ*, 469, 480
- Kravtsov, A. V., Vikhlinin, A., & Nagai, D. 2006, *ApJ*, 650, 128
- Lacey, C., & Cole, S. 1993, *MNRAS*, 262, 627
- Lemson, G., & Springel, V. 2006, in *Astronomical Data Analysis Software and Systems XV*, ed. C. Gabriel, C. Arviset, D. Ponz, & E. Solano (San Francisco: ASP Conf. Ser. 351), 212
- Loken, C., Norman, M. L., Nelson, E., Burns, J., Bryan, G. L., & Motl, P. 2002, *ApJ*, 579, 571
- Lukić, Z., Heitmann, K., Habib, S., Bashinsky, S., & Ricker, P. M. 2007, *ApJ*, 671, 1160
- McNamara, B. R., Nulsen, P. E. J., Wise, M. W., Rafferty, D. A., Carilli, C., Sarazin, C. L., & Blanton, E. L. 2005, *Nature*, 433, 45
- Motl, P. M., Hallman, E. J., Burns, J. O., & Norman, M. L. 2005, *ApJ*, 623, L63
- Nagai, D. 2006, *ApJ*, 650, 538
- Navarro, J. F., Frenk, C. S., & White, S. D. M. 1997, *ApJ*, 490, 493
- Percival, W. J. 2005, *A&A*, 443, 819
- Poole, G. B., Babul, A., McCarthy, I. G., Fardal, M. A., Bildfell, C. J., Quinn, T., & Mahdavi, A. 2007, *MNRAS*, 678
- Poole, G. B., Fardal, M. A., Babul, A., McCarthy, I. G., Quinn, T., & Wadsley, J. 2006, *MNRAS*, 373, 881
- Press, W. H., & Schechter, P. 1974, *ApJ*, 187, 425
- Randall, S. W., Sarazin, C. L., & Ricker, P. M. 2002, *ApJ*, 577, 579 (RSR)
- Reid, B. A., & Spergel, D. N. 2006, *ApJ*, 651, 643
- Rephaeli, Y. 1995, *ARA&A*, 33, 541
- Ricker, P. M., & Sarazin, C. L. 2001, *ApJ*, 561, 621, (RS)
- Ritchie, B. W., & Thomas, P. A. 2002, *MNRAS*, 329, 675
- Sarazin, C. L. 2002, in *Merging Processes in Galaxy Clusters*, ed. L. Feretti, I. M. Gioia, & G. Giovannini (Dordrecht: Kluwer), 1
- Sheth, R. K., & Tormen, G. 1999, *MNRAS*, 308, 119
- Springel, V., et al. 2005, *Nature*, 435, 629
- Sunyaev, R. A., & Zel’dovich, Y. B. 1972, *Comments on Astrophysics and Space Physics*, 4, 173
- Vikhlinin, A., Kravtsov, A., Forman, W., Jones, C., Markevitch, M., Murray, S. S., & Van Speybroeck, L. 2006, *ApJ*, 640, 691
- Wang, L., & Steinhardt, P. J. 1998, *ApJ*, 508, 483
- Weller, J., Battye, R. A., & Kneissl, R. 2002, *Phys. Rev. Lett.*, 88, 1301

APPENDIX

FITTING SIMULATION DATA

We use the same basic forms and procedures to fit the merger boosts discussed in RSR, Appendix B. For the integrated Comptonization parameter, the boosted part of the cumulative time distribution histograms is well-fit by

TABLE 2
MERGER-INDUCED SZ- M RELATIONS AND SCATTER

	Model	z	σ_{eq}	σ_{fit}	A_{nb}	A_{b}	α_{nb}	α_{b}
Y	Flat	0.0	0.0205	0.0218	12.0	11.9	1.91	1.91
		0.5	0.0190	0.0205		11.9		1.91
		1.0	0.0197	0.0212		11.9		1.91
	Open	0.0	0.0207	0.0220	12.0	11.9	1.91	1.91
		0.5	0.0191	0.0207		11.9		1.91
		1.0	0.0203	0.0216		11.9		1.91
	EdS	0.0	0.0214	0.0228	12.0	11.9	1.91	1.91
		0.5	0.0194	0.0209		11.9		1.91
		1.0	0.0222	0.0235		11.9		1.91
y_{max}	Flat	0.0	0.292	0.241	8.25	9.01	1.24	1.26
		0.5	0.361	0.271		9.39		1.27
		1.0	0.412	0.289		9.70		1.27
	Open	0.0	0.293	0.246	8.25	8.96	1.24	1.26
		0.5	0.329	0.256		9.20		1.27
		1.0	0.375	0.279		9.46		1.26
	EdS	0.0	0.414	0.290	8.25	9.72	1.24	1.27
		0.5	0.485	0.301		10.3		1.27
		1.0	0.531	0.299		10.7		1.28

TABLE 3
BEST-FIT VALUES FOR Ω_M AND σ_8 FOR THREE WORLD MODELS

	Model	z	Boosts?	Ω_M	Difference	σ_8	Difference	
Y	Flat	0,0.5	no	0.287		0.857		
			yes	0.289	0.7%	0.854	-0.4%	
		0,1.0	no	0.277		0.865		
			yes	0.277	0.0%	0.865	0.0%	
		Open	0,0.5	no	0.278		0.857	
				yes	0.279	0.4%	0.856	-0.1%
	0,1.0	no	0.279		0.855			
		yes	0.280	0.4%	0.855	0.0%		
	EdS	0,0.5	no	0.932		0.531		
			yes	0.931	-0.1%	0.531	0.0%	
		0,1.0	no	0.874		0.541		
			yes	0.873	-0.1%	0.541	0.0%	
y_{max}		Flat	0,0.5	no	0.295		0.844	
				yes	0.199	-33%	1.020	21%
	0,1.0	no	0.267		0.870			
		yes	0.229	-14%	0.976	12%		
	Open	0,0.5	no	0.282		0.848		
			yes	0.213	-24%	0.984	16%	
0,1.0	no	0.281		0.848				
	yes	0.236	-16%	0.954	13%			
EdS	0,0.5	no	0.953		0.524			
		yes	0.921	-3.4%	0.589	12%		
0,1.0	no	0.905		0.532				
	yes	0.924	2.1%	0.590	11%			

TABLE 4
BEST-FIT FLAT WORLD MODELS WITH CONSTANT w

	z	Boosts?	Ω_M	Difference	σ_8	Difference	w	Difference
Y	0,0.5	no	0.314		0.837		-0.879	
		yes	0.316	0.6%	0.835	-0.2%	-0.885	0.7%
	0,1.0	no	0.275		0.874		-1.062	
		yes	0.271	-1.5%	0.877	0.3%	-1.080	1.7%
y_{max}	0,0.5	no	0.324		0.823		-0.861	
		yes	0.173	-47%	1.082	24%	-1.255	46%
	0,1.0	no	0.279		0.863		-0.987	
		yes	0.192	-31%	1.045	21%	-1.240	26%

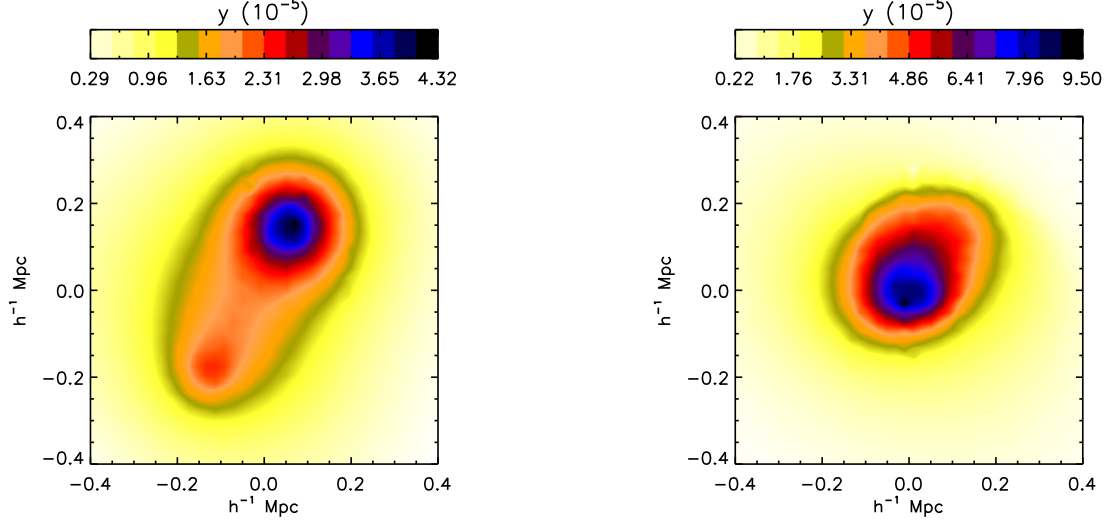


FIG. 1.— Images of the SZ parameter y from 3D snapshots of the 1:3 mass ratio, $2 r_s$ impact parameter merger simulation. Here r_s is the NFW scale radius of the more massive cluster. Both images are viewed from a line-of-sight which is rotated 45° from the merger axis and 45° azimuthally from the merger plane. *Left*: 386 Myr before first core crossing. *Right*: 114 Myr after first core crossing.

hyperbolae similar in form to equation (B1) of RSR with a slight modification:

$$\ln\left(\frac{t}{t_{\text{sc}}}\right) = \sqrt{\left(\left\{\frac{Y}{Y(0)} - \left[\frac{Y}{Y(0)}\right]_{\text{peak}} - 1\right\}^2 - 1\right)} (\epsilon^2 - 1) - \ln\left(\frac{t}{t_{\text{sc}}}\right)_Y. \quad (\text{A1})$$

Three parameters describe the function: the maximum boost $[Y/Y(0)]_{\text{peak}}$, the boost duration $(t/t_{\text{sc}})_Y$, and the eccentricity of the hyperbola ϵ . The fit values for these parameters between simulation runs could be reproduced with the same functions of fractional mass increase f_M and normalized impact parameter b' used in RSR, provided here for completeness:

$$\left[\frac{Y}{Y(0)}\right]_{\text{peak}}(f_M, b') = \frac{A f_M^B}{C + b'^2} + 1, \quad (\text{A2})$$

$$\epsilon(f_M, b') = \left(\frac{A f_M^B}{C + b'^2}\right), \quad (\text{A3})$$

$$\ln\left(\frac{t}{t_{\text{sc}}}\right)_Y = G \frac{\ln(M_{<} + M_{>}) - H \ln(M_{<}^{1/3} + M_{>}^{1/3})}{I + b'^2}. \quad (\text{A4})$$

As in the text, the impact parameter is scaled by the core radii of the two merging clusters, $b' = b/(r_{c<} + r_{c>})$, $M_{<}$ and $M_{>}$ are the masses of the less massive and more massive cluster (in M_\odot), respectively, and the fractional mass increase $f_M \equiv M_{<}/(M_{<} + M_{>})$. Motivations for these forms are given in Appendix B of RSR.

The variation of y_{max} with the viewing angle of the merger causes the histograms of values of time versus y_{max} to be broader than the histograms for Y (Figure 3). This difference makes hyperbolae a poor representation of the histogram shapes. We find a suitable replacement in another 3 parameter function

$$\ln\left(\frac{t}{t_{\text{sc}}}\right) = P \ln\left(1 - \frac{y_{\text{max}}}{y_{\text{peak}}}\right) - \frac{1}{2} \frac{y_{\text{max}}}{y_{\text{peak}}} - \ln\left(\frac{t}{t_{\text{sc}}}\right)_y, \quad (\text{A5})$$

with similarly defined parameters for the maximum y_{max} boost $\frac{y_{\text{peak}}}{y_{\text{max}}(0)}$, the power law slope P , and the boost duration $\ln\left(\frac{t}{t_{\text{sc}}}\right)_y$:

$$\frac{y_{\text{peak}}}{y_{\text{max}}(0)} = \frac{A f_M^B}{C + b'^{1.3}} + 1, \quad (\text{A6})$$

$$P = \left(\frac{D}{F + b'^{1.5}}\right)^{-1}, \quad (\text{A7})$$

$$\ln\left(\frac{t}{t_{\text{sc}}}\right)_y = G \frac{\ln(M_{<} + M_{>}) - H \ln(M_{<}^{1/3} + M_{>}^{1/3})}{I + b'^2}. \quad (\text{A8})$$

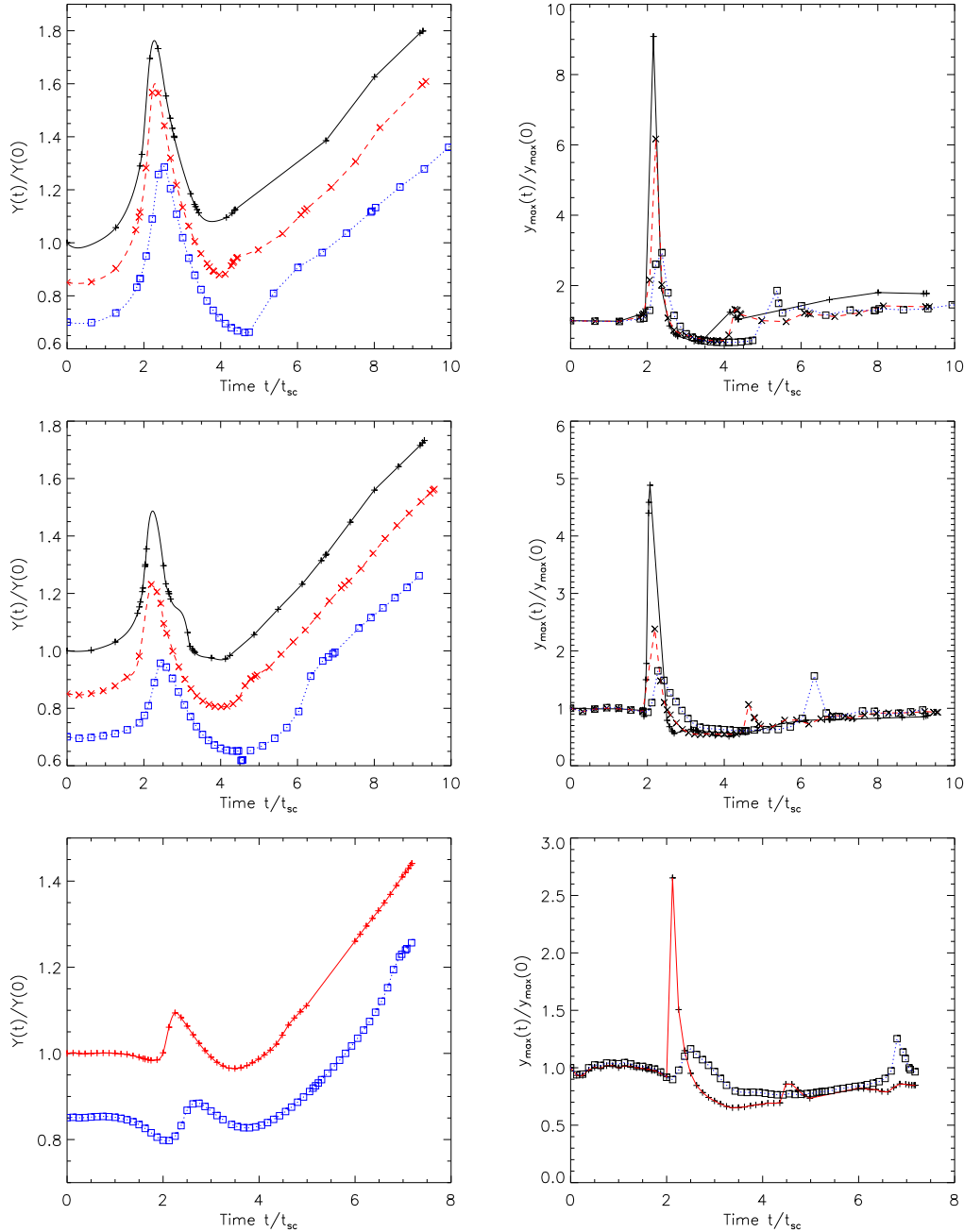


FIG. 2.— Evolution of the SZ effect during a merger. In each panel, different curves are for different values of the merger impact parameter: $b = 0$ (solid, black line), $2 r_s$ (dashed, red line), and $5 r_s$ (dotted, blue line), where r_s is the NFW scale radius of the more massive cluster. In the left panels, the $b = 2 r_s$ simulation run is offset downward by 0.15 and the $5 r_s$ run is offset downward by 0.3 for clarity. The time is scaled by the sound crossing time t_{sc} of the more massive premerger cluster. *Left*: Integrated Comptonization parameter Y versus time for the 1:1 (top), 1:3 (middle), and 1:6.5 (bottom) mass ratios. *Right*: Maximum Comptonization parameter y_{max} versus time for the 1:1 (top), 1:3 (middle), and 1:6.5 (bottom) mass ratios. The mergers are observed 90° to the merger axis and in the merger plane.

The best-fit values found for A – I are given in Table 5. Note that A – I are found assuming that the value of $y_{max}(0)$ is taken along the merger axis, which is twice the value of $y_{max}(0)$ used in Figures 2 and 3, for which the value perpendicular to the merger axis is used.

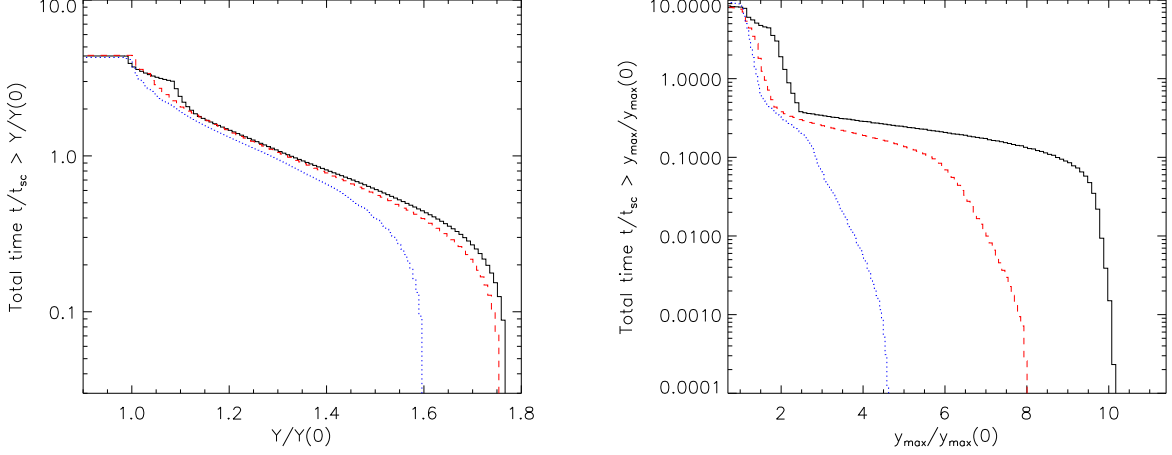


FIG. 3.— *Left*: Histogram of the total time the integrated Comptonization parameter Y is above some fraction of its initial premerger value $Y(0)$, scaled by the sound crossing time t_{sc} of the more massive premerger cluster. Histograms are shown for equal-mass mergers at 3 impact parameters $b = 0$ (solid, black line), $2 r_s$ (dashed, red line), $5 r_s$ (dotted, blue line), where r_s is the NFW scale radius of the more massive cluster. *Right*: Histogram of times for y_{max} .

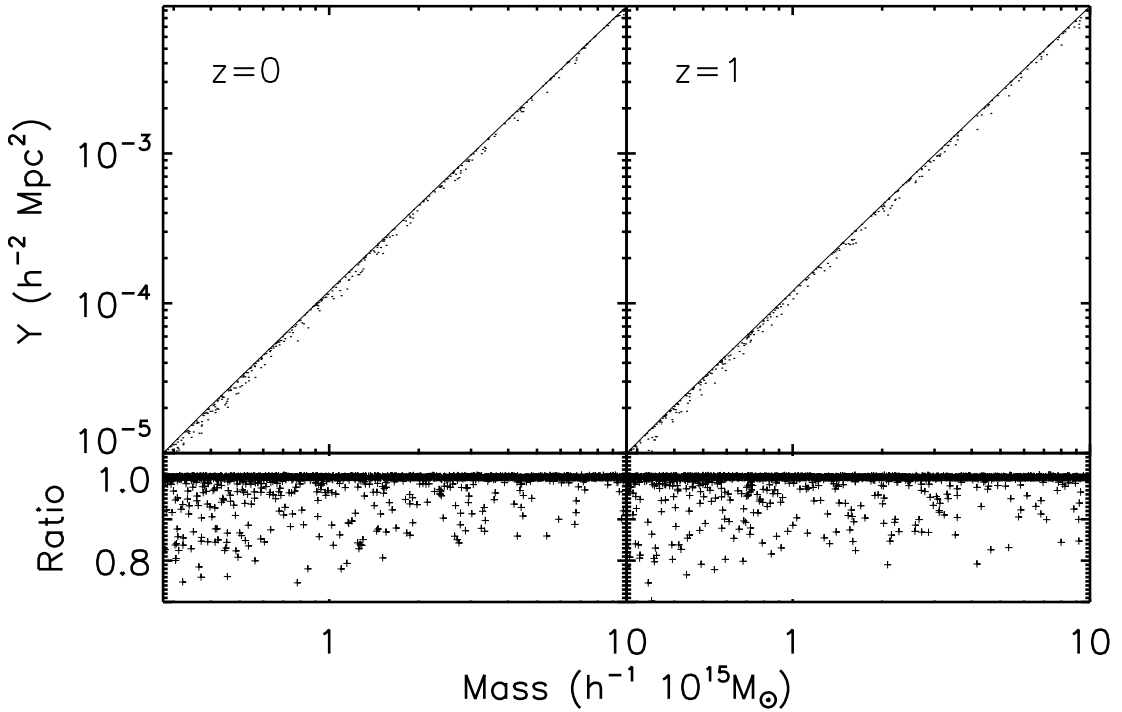


FIG. 4.— Integrated Comptonization parameter Y (*top panels*) versus total mass in the flat cosmology at $z = 0$ (*left panels*) and $z = 1$ (*right panels*) for clusters with $Y > 10^{-5} h^{-2} \text{Mpc}^2$. The combined mass of both merging clusters is used if Y is boosted or $t_{obs} > t_{merge}$, where t_{merge} is the time of maximum boost. The apparent solid line is the result of many individual clusters at or near their equilibrium values of Y . In the *bottom panels*, the ratio of the boosted clusters to their equilibrium values for each redshift is shown. Each panel contains 5190 clusters.

TABLE 5
FITTING PARAMETERS FOR MERGER BOOST HISTOGRAMS

Boost	A	B	C	D	E	F	G	H	I
$Y/Y(0)$	95.69	0.8793	66.72	94.83	0.3621	173.3	33.36	0.2793	473.3
$y_{max}/y_{max}(0)$	26.55	0.5776	4.052	6.310	-	4.569	2.250	1.785	13.76

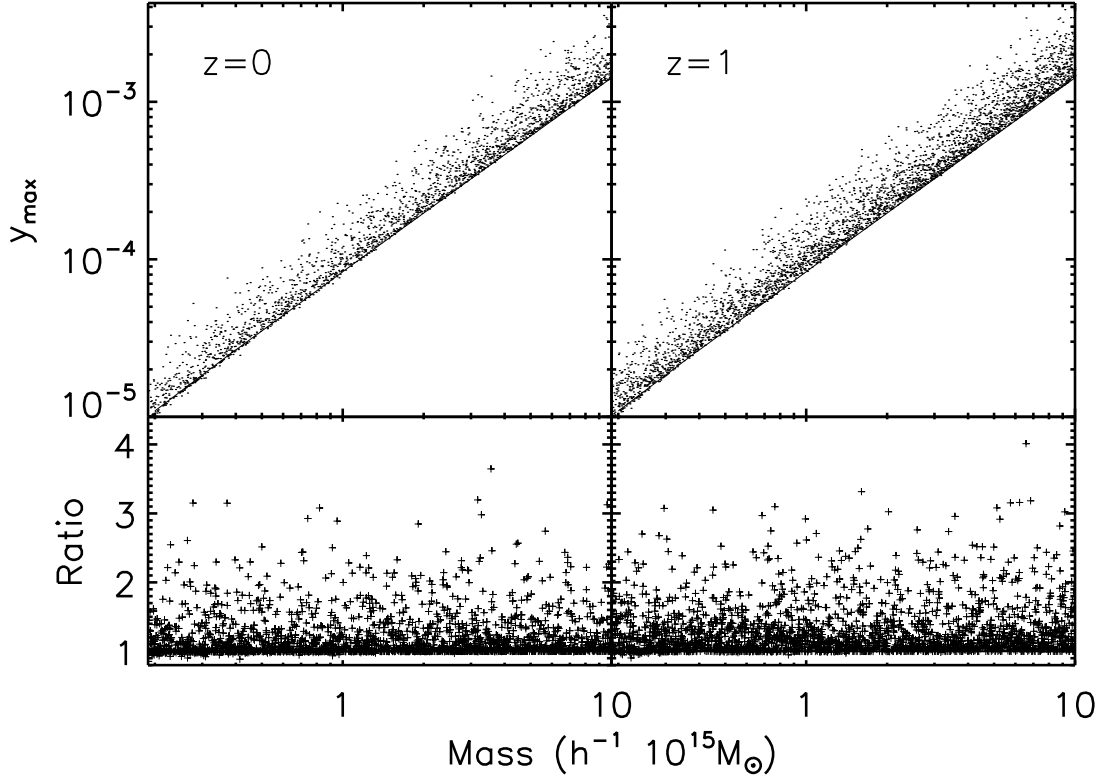


FIG. 5.— Same as Figure 4, but for the maximum Comptonization parameter y_{\max} , for clusters with $y_{\max} > 10^{-5}$. Each panel contains 5663 clusters.

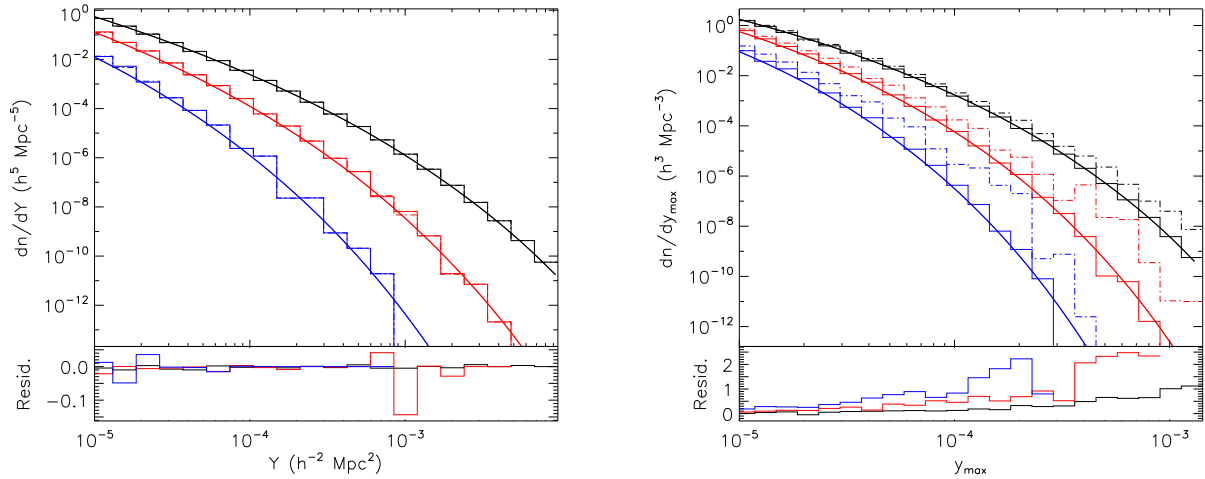


FIG. 6.— Boosted (*dashed line*) versus nonboosted (*solid line*) integrated Comptonization parameter function YF (*left panel*) and maximum Comptonization parameter function yF (*right panel*) histograms for $z = 0$ (*top, black*), $z = 0.5$ (*middle, red*), and $z = 1$ (*bottom, blue*) in the flat universe. The smooth curves are the analytic PS predictions at each redshift given by equation (7). The residual plots give the difference in the logs between the boosted and nonboosted YF s and yF s. Note the significant difference in scales of the residuals between the YF s and yF s.